Preparation of Thick Amorphous Alloy Sheets in Multicomponent Fe-based Systems and Their Thermal and Magnetic Properties

Sci. Rep. RITU A43 (1997) pp. 115-121
No. 2, March 1997

Preparation of Thick Amorphous Alloy Sheets in Multicomponent Fe-based Systems and Their Thermal and Magnetic Properties *

Akihisa INOUE[a], Takao MIZUSHIMA[b] and Akihiro MAKINO[b]

[a] *Institute for Materials Research, Tohoku University, Sendai 980-77, Japan*
[b] *Central Research Laboratory, Alps Electric Co. Ltd., Nagaoka 940, Japan*

(Received January 14, 1997)

Thick amorphous sheets with thickness up to about 200 μm were formed for the $Fe_{72}Al_5Ga_2P_{10}C_6B_4Si_1$ alloy with a wide supercooled liquid region of 58 K before crystallization. The glass transition temperature (T_g), crystallization temperature (T_x) and supercooled liquid region $\Delta T_x(=T_x-T_g)$ remain unchanged in the entire thickness range. However, the heat of structural relaxation decreases from 2.2 kJ/mol for the 22 μm thick ribbon to 0.48 kJ/mol for the 160 μm thick ribbon, accompanying the increase in T_c from 597 K to 619 K. In comparison with the other amorphous alloy ribbons in the same Fe-(Al,Ga)-(P,C,B,Si) system, there is a clear tendency for the maximum sample thickness for glass formation (t_{max}) to increase with increasing ΔT_x. The Fe-Al-Ga-P-C-B-Si amorphous sheets have high saturation magnetization of about $180x10^{-6}$ Wbm/kg and low coecivity of about 5 A/m in the annealed state and their values remain unchanged in the thickness range up to 200 μm. The permeability (μ_e) at 1 kHz shows the high values of 12000 for the 30 μm thick ribbon and decreases to about 7000 for the 200 μm thick ribbon. It is to be noticed that the good soft magnetic properties of 5 A/m for H_c and 7000 for μ_e as well as the wide supercooled liquid region of 58 K are obtained for the thick amorphous sheets with thickness of 150 to 200 μm. These characteristics for the thick amorphous ribbons have not been obtained for Fe-based amorphous alloys previously reported. It is therefore expected that the thick amorphous ribbons cause a further extension of the application fields of ferromagnetic amorphous alloys.

KEYWORDS: ferromagnetic glassy alloy, rapid solidification, wide supercooled liquid region, soft-magnetic property, sample thickness

1. Introduction

Since the findings of good soft magnetic properties for Fe-based amorphous alloys[1][2], the appearance of ferromagnetic bulk amorphous alloys has been desired for the last three decades. Recently, a number of bulk amorphous alloys with a sample diameter above 1 mm have been synthesized in Mg-Ln-TM[3][4], Ln-Al-TM[5][6], Zr-Al-TM[7][8], Zr-Ti-TM-Be[9] and Pd-Cu-Ni-P[10] (Ln=lanthanide metal, TM=transition metal) systems. The critical cooling rate for glass formation for these bulk amorphous alloys is in the range from 0.10 to 100 K/s[11]-[13] and the maximum sample thickness is as large as 72 mm[14]. However, these bulk amorphous alloys found before 1994 had been limited to nonferrous metal base systems without ferromagnetism at room temperature. The three empirical rules for the achievement of large glass-forming ability has been derived[11]-[13][15] on the basis of the above-described multicomponent bulk amorphous alloys. That is, (1) multicomponent alloy systems consisting of more than three elements, (2) large atomic size ratios above about 12 % among the main constituent elements, and (3) negative heats of mixing. According to the three empirical rules, we have searched a new bulk amorphous alloy in Fe-based system. As a result, Fe-based bulk amorphous alloys with a diameter up to 2 mm were found[16]-[18] to be formed by copper mold casting in Fe-(Al,Ga)-(P,C,B,Si) system where the three group elements satisfy the three empirical rules. By using the new Fe-based alloy compositions with large glass-forming ability, it is expected that thick amorphous Fe-based alloy sheets are prepared even by the melt spinning technique. The trial of producing a thick amorphous sheet in Fe-based system is important for further extension of application fields for ferromagnetic amorphous alloys. This paper is intended to examine the changes in the structure, thermal stability and magnetic properties as a function of sample thickness for melt-spun $Fe_{72}Al_5Ga_2P_{10}C_6B_4Si_1$ alloy sheets and to investigate the possibility of producing a thick amorphous alloy sheet with good soft magnetic properties.

*IMR Report No.2069

2. Experimental Procedure

Multicomponent alloys with composition $Fe_{73}Al_5Ga_2P_{11-x}C_5B_4Si_x$ and $Fe_{72}Al_5Ga_2P_{11-x}C_6B_4Si_x$ (x=0 and 1 at%) were used because the $Fe_{72}Al_5Ga_2P_{11}C_6B_4$ alloy was one of Fe-based amorphous alloys with a wide supercooled liquid region exceeding 50 K[19]. Their alloy ingots were prepared by induction melting the mixture of pure Fe, Al and Ga metals, premelted Fe-P and Fe-C alloys and pure B and Si crystals in an argon atmosphere. Rapidly solidified alloy ribbons with various thicknesses ranging from 15 to

230 μm were prepared by controlling the rotation speed of wheel with a single roller melt-spinning equipment. The amorphous nature was examined by X-ray diffraction and optical and transmission electron microscopy (OM and TEM). The distribution of alloy components was measured by energy dispersive X-ray (EDX) spectroscopy. Thermal stability associated with structural relaxation, glass transition, supercooled liquid region and crystallization was examined at a heating rate of 0.67 K/s by differential scanning calorimetry (DSC). Magnetic properties of saturation magnetization, coercivity and permeability at 1 kHz were measured at room temperature with a vibrating sample magnetometer (VSM), a B-H loop tracer and an impedance analyzer, respectively.

3. Results

3.1. Formation of thick amorphous sheets

Figure 1 shows the X-ray diffraction patterns taken from the freely solidified surface in the melt-spun $Fe_{72}Al_5Ga_2P_{10}C_6B_4Si_1$ sheets with different thicknesses ranging from 22 to 220 μm. The change in the sheet thickness was achieved by controlling the wheel velocity, nozzle diameter and ejection pressure etc. The sheet samples with thicknesses below 160 μm consist only of a broad peak at a wave vector ($K_p=4\pi\sin\theta/\lambda$) of about 31 nm^{-1}. However, the further increase in the sheet thickness to 220 μm causes the formation of coexistent amorphous and Fe_3B phases. It is therefore concluded that the critical sample thickness for glass formation by the conventional melt spinning method lies around 200 μm. It is to be noticed that the critical thickness is much larger than the maximum value (≅ 70 to 100 μm) for Fe-Si-B amorphous alloys. In order to clarify the size and distribution state of the crystalline Fe_3B phase, the bright-field electron micrographs and selected-area electron diffraction patterns taken from the regions near the freely solidified and roll-contacted surfaces are shown in Fig. 2 (a) and (b) for the 160 μm thick sheet and in Fig. 3 (a) and (b) for the 220 μm thick sheet. No appreciable crystalline phase is seen on both surfaces for the 160 μm thick sheet. However, fine Fe_3B precipitates with a size of about 10 nm are embedded only in an amorphous phase near the freely solidified surface, though the amorphous phase is a main constituent phase for the 220 mm thick sheet. On the other hand, the region near the roll-contacted surface keeps an amorphous phase without crystallinity. The preferential precipitation of the Fe_3B phase on the freely solidified surface is due to the lower cooling rate as compared with that on the roll-contacted surface because the heat release in the single roller melt spinning technique is made through the contact with the copper wheel. With the aim of confirming whether or not the partial crystallization is due to the segregation of the constituent elements along the direction of sample thickness, the EDX analyses were made on the freely solidified and roll-controlled surfaces for the 160 μm thick sheet. As shown in Fig. 4, there is no appreciable difference in the peak intensity and peak position for all the constituent elements and hence all the elements distribute homogeneously over the entire sample thickness. The absence of solute segregation along the direction of thickness also supports the presumption that the partial

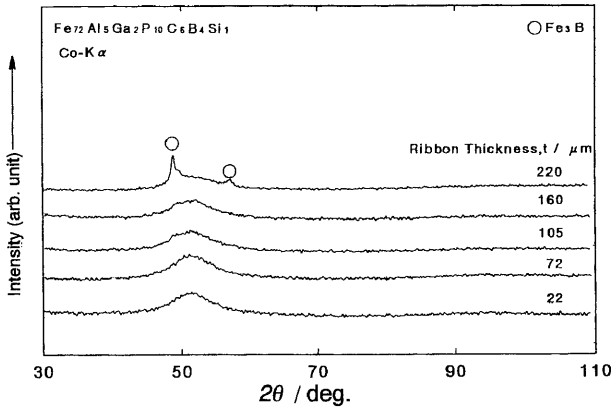

Figure 1. X-ray diffraction patterns of $Fe_{72}Al_5Ga_2P_{10}C_6B_4Si_1$ alloy sheets with various thicknesses of 22 to 220 μm prepared at different circumferential velocities of 2 to 30 m/s by the single roller melt-spinning method.

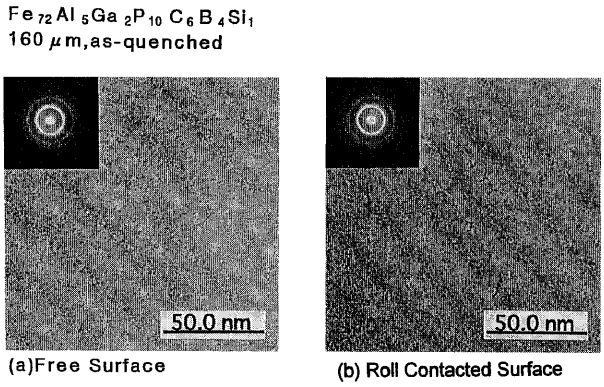

Figure 2. Bright-field electron micrographs and selected-area electron diffraction patterns of the melt-spun $Fe_{72}Al_5Ga_2P_{10}C_6B_4Si_1$ alloy ribbon with a thickness of 160 μm. (a) free surface, (b) roll-contacted surface.

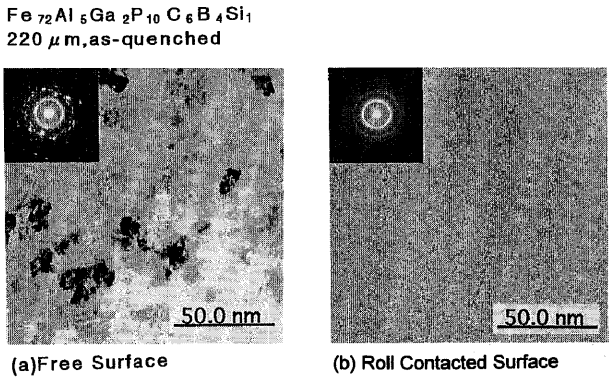

Figure 3. Bright-field electron micrographs and selected-area electron diffraction patterns of the melt-spun $Fe_{72}Al_5Ga_2P_{10}C_6B_4Si_1$ alloy ribbon with a thickness of 220 μm. (a) free surface, (b) roll-contacted surface.

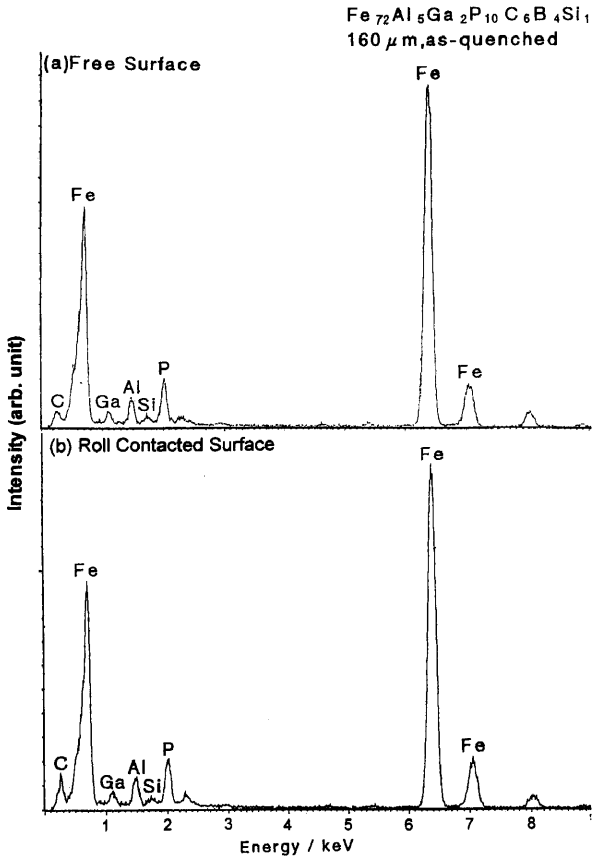

Figure 4. EDX profiles of the melt-spun $Fe_{72}Al_5Ga_2P_{10}C_6B_4Si_1$ alloy ribbon with a thickness of 160 μm. (a) free surface, (b) roll-contacted surface.

precipitation of the Fe_3B phase only on the freely solidified surface is due to the lower cooling rate.

3-2. Thermal stability

Figure 5 shows the DSC curves of the melt-spun Fe-Al-Ga-P-C-B-Si sheets with the thicknesses of 22, 72, 160 and 220 μm. Although the glass transition temperature (T_g) remains constant in the entire thickness range, the onset temperature of crystallization (T_x) keeps a constant value in the thickness range up to 160 μm and then decreases slightly for the 220 μm thick sheet. However, no appreciable change in the single-stage exothermic peak behavior is seen, indicating that the 220 μm thick sheet consists mainly of an amorphous phase. The small endothermic peak marked with an arrow is due to the transition from ferromagnetism to paramagnetism. There is a tendency for the Curie temperature (T_c) to increase with increasing sample thickness. Based on the DSC curves exemplified in Fig. 5, the T_x, T_g and $\Delta T_x(=T_x-T_g)$ as a function of sheet thickness for $Fe_{72}Al_5Ga_2P_{11}C_6B_4$, $Fe_{72}Al_5Ga_2P_{10}C_6B_4Si_1$, $Fe_{73}Al_5Ga_2P_{11}C_5B_4$ and $Fe_{73}Al_5Ga_2P_{10}C_5B_4Si_1$ amorphous alloys are plotted in Fig. 6. The T_g values are nearly constant over the entire ribbon thickness, while the T_x decreases in the thickness range above about 200 μm, leading to the decrease in ΔT_x in the large thickness range.

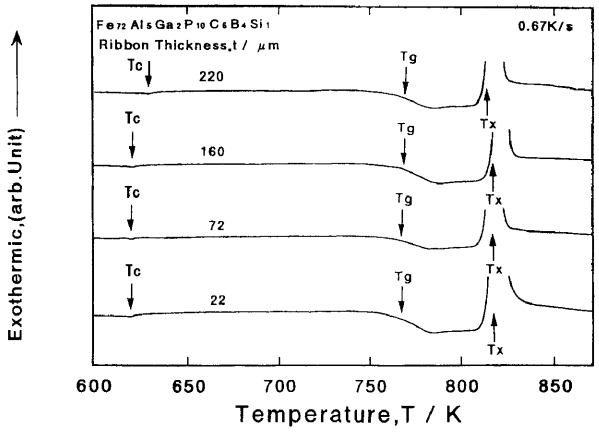

Figure 5. DSC curves of the melt-spun $Fe_{72}Al_5Ga_2P_{10}C_6B_4Si_1$ alloy ribbons with different thicknesses of 22, 72, 160 and 220 μm. The T_c, T_g and T_x represent the Curie temperature, glass transition temperature and onset temperature of crystallization, respectively.

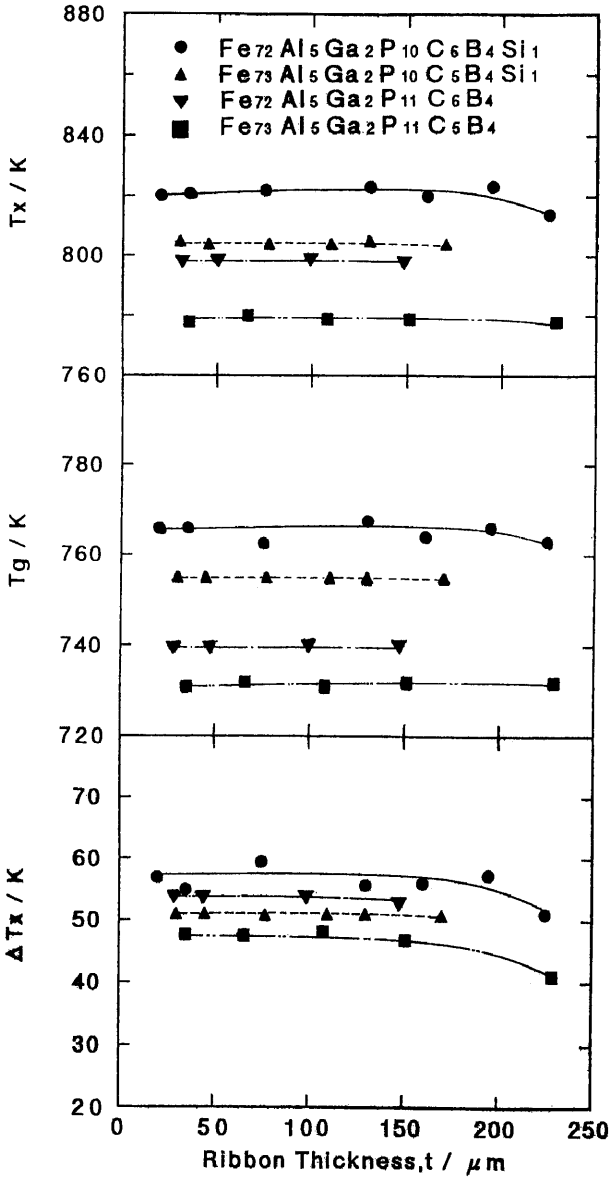

Figure 6. Changes in T_x, T_g and $\Delta T_x(=T_x-T_g)$ with ribbon thickness for multicomponent Fe-based amorphous alloys.

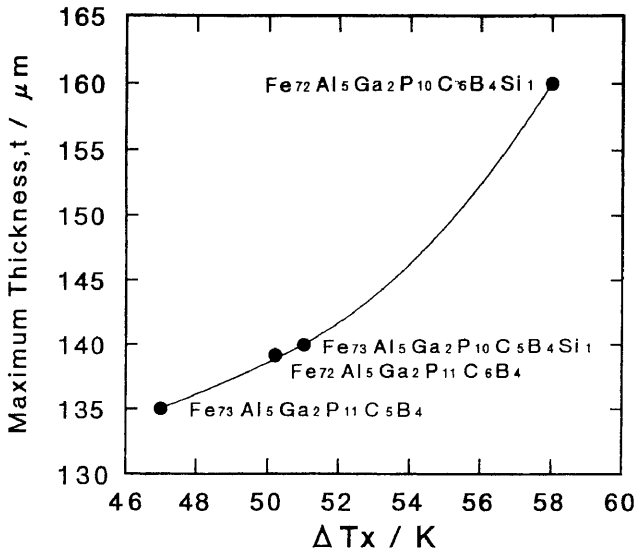

Figure 7. Relation between the maximum sample thickness (t_{max}) and the temperature interval of supercooled liquid region (ΔT_x) for the multicomponent Fe-based amorphous alloys.

This result indicates that the thermal stability of the supercooled liquid remains almost unchanged in the thickness range below about 200 μm. Figure 7 shows the relation between the maximum sheet thickness for glass formation (t_{max}) and the temperature interval of the supercooled liquid region ($\Delta T_x=T_x-T_g$) for the Fe-based amorphous alloys. There is a clear tendency for t_{max} to increase with increasing ΔT_x. The large glass-forming ability for the present Fe-based alloys is concluded to originate from the high thermal stability of the supercooled liquid against crystallization.

3.3. Magnetic properties

Figure 8 shows the hysteresis B-H loops of the melt-spun $Fe_{72}Al_5Ga_2P_{10}C_6B_4Si_1$ amorphous sheets with thicknesses of 30, 70 and 160 μm in as-quenched and annealed (1.8 ks, 623 K) states. Although the coercivity decreases by annealing, there is no distinct change in the hysteresis loop behavior with sheet thickness. Based on the data of the B-H loops, the saturation magnetization (σ_s), coercivity (H_c) and permeability (μ_e) at 1 kHz as a function of sheet thickness for the $Fe_{72}Al_5Ga_2P_{10}C_6B_4Si_1$ amorphous sheets in the as-quenched and annealed states are plotted in Fig. 9. It is clearly seen that the annealing causes a significant improvement of soft magnetic properties, i.e., the decrease in H_c from about 10 A/m to about 5 A/m and the increase in μ_e from about 6000 to 7000-12000, though the σ_s remains almost constant. Besides, as the sheet thickness increases, the σ_s and H_c change slightly, but the μ_e decreases significantly from 12000 to 7000. The degradation of μ_e is presumably due to the increase in the influence of demagnetization resulting from the increase in the area of the lateral side.

Figure 10 summarizes the changes in H_c, μ_e at 1 kHz and annealed structure with ribbon thickness for the

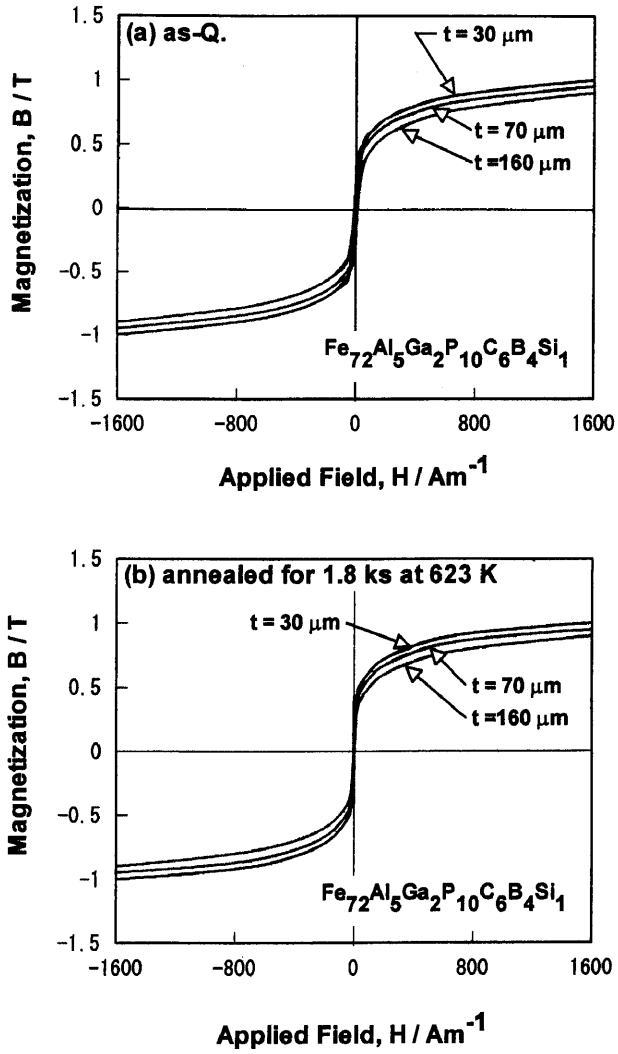

Figure 8. Hysteresis B-H loops of the melt-spun $Fe_{72}Al_5Ga_2P_{10}C_6B_4Si_1$ alloy ribbons with various thicknesses of 30, 70 and 160 μm.

$Fe_{72}Al_5Ga_2P_{10}C_6B_4Si_1$ and $Fe_{72}Al_5Ga_2P_{11}C_6B_4$ alloys, together with the data[20][21] of a conventional $Fe_{78}Si_9B_{13}$ alloy. It is seen that the new Fe-based amorphous alloys keep good soft magnetic properties with H_c below about 5 A/m and μ_e above 7000. Although the soft magnetic properties in the thickness range below 100 μm are nearly the same as those for the Fe-Si-B alloy, a further increase in the ribbon thickness to above 100 μm causes a significant difference in the soft magnetic properties. That is, the Fe-Si-B amorphous alloy does not have high μ_e and only the new Fe-based amorphous alloys can keep good soft magnetic properties of about 5 A/m for H_c and above 7000 for μ_e. Considering that only the new Fe-based amorphous alloys have a wide supercooled liquid region reaching about 50 to 60 K before crystallization, it is expected that the thick amorphous sheets are rather easily consolidated into a bulk amorphous form with full density and the bulk amorphous alloy keeps the same good soft magnetic properties as those for the thick amorphous sheets. The Fe-Si-B amorphous alloys do not have the supercooled liquid region before crystallization and hence the consolidation into a bulk form by utilizing the large

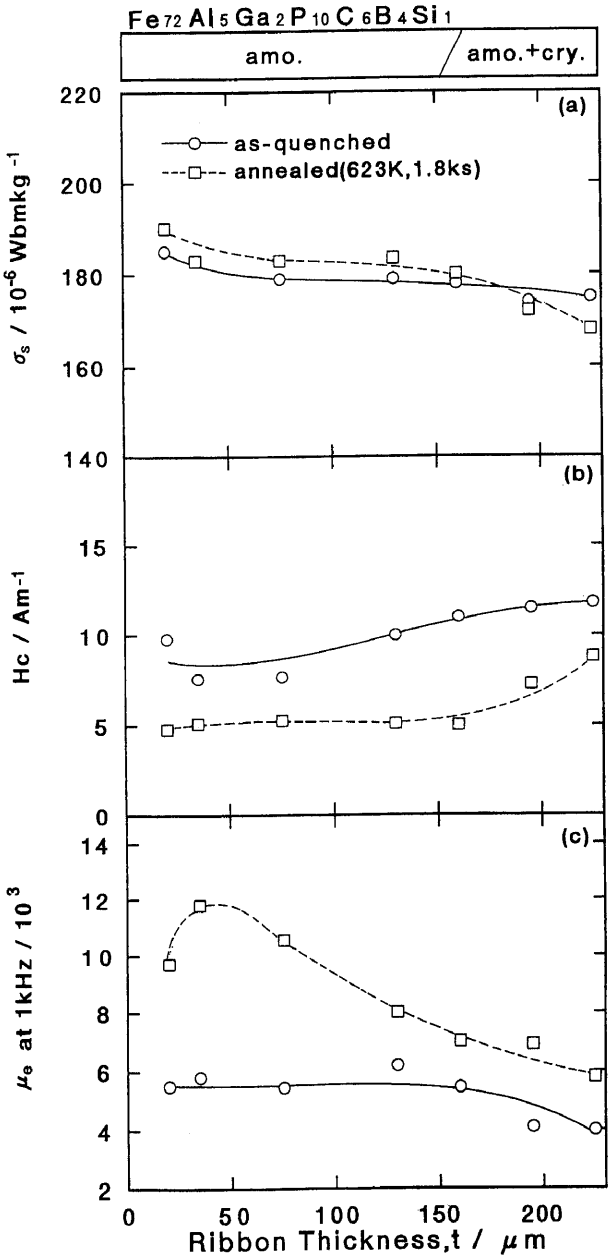

Figure 9. Changes in σ_s, H_c, μ_e and annealed structure with ribbon thickness for the melt-spun $Fe_{72}Al_5Ga_2P_{10}C_6B_4Si_1$ alloy ribbons.

viscous flow is difficult. The difficulty may be the reason for the unsuccessful results for the formation of a bulk amorphous alloy with good soft magnetic properties.

4. Discussion

4.1. Difference in the maximum sample thickness for glass formation between the cast and the melt-spun alloys

It has previously been reported that the use of the copper mold casting method causes the formation of bulk amorphous alloys with diameters of about 1 mm for the $Fe_{72}Al_5Ga_2P_{11}C_6B_4$ alloy[16] and about 2 mm for the

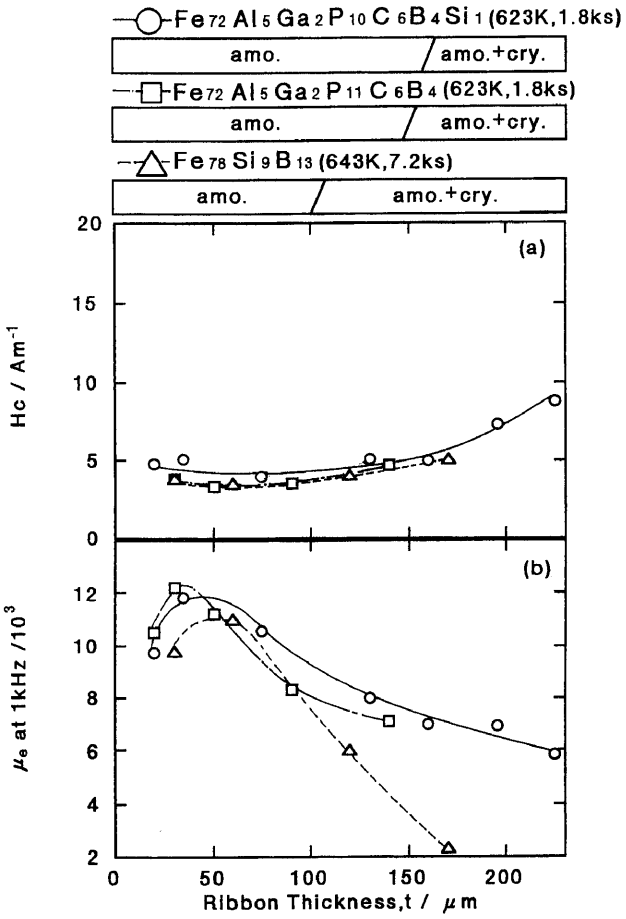

Figure 10. Changes in H_c, μ_e and annealed structure with ribbon thickness for the melt-spun $Fe_{72}Al_5Ga_2P_{10}C_6B_4Si_1$ and $Fe_{72}Al_5Ga_2P_{11}C_6B_4$ alloy ribbons. The data of an amorphous $Fe_{78}Si_9B_{13}$ ribbon are also shown for comparison.

$Fe_{72}Al_5Ga_2P_{10}C_6B_4Si_1$ alloy[17][18]. These maximum diameters are much larger than the largest thickness (150 to 180 μm) for the thick amorphous sheets prepared by melt spinning, in spite of the same alloy compositions. The significant difference in the maximum sample thickness is due to the difference in the released method of heat. That is, the single roller melt spinning method is eliminated mainly from the wheel which is contacted with the molten alloy. Furthermore, the contacting time of the molten alloy with the rotating wheel is as short as about 0.006 to 0.8 s. On the other hand, the molten alloy cast into the inner cylindrical cavity of the copper mold is cooled to room temperature through the release of heat from all the surrounding area which is contacted with copper mold. The difference suggests that the efficiency of cooling for the molten alloy is much greater for the copper mold casting process than for the single roller melt spinning process. The higher efficiency of the cooling seems to cause the formation of the amorphous alloy with the diameters up to 2 mm which is much larger than the maximum thickness (0.2 mm) of the melt-spun amorphous ribbon.

4.2. Difference in the maximum sample thickness for glass formation by the difference in the melt spinning techniques

It has previously been reported that the use of the special melt spinning technique in which the rotating wheel at a high circumferential velocity of 60 m/s can be stopped within a short time of 1 to 2 s causes the formation of an amorphous ribbon with a maximum thickness up to 250 μm for $Fe_{75}Si_{10}B_{15}$[22], 190 μm for $Fe_{80}P_{13}C_7$[23] and 160 μm for $Co_{72.5}Si_{12.5}B_{15}$[24]. The resulting samples have continuously different thicknesses in the range from 15 to 300 μm depending on the rotation speed of 6000 to 500 rpm. In the special melt spinning method, the good contacting state between the molten alloy and the copper wheel is first obtained at the high rotation speed of 6000 rpm and enables highly efficient release of heat, leading to the formation of the much thicker amorphous ribbons. These maximum thicknesses are much larger than the maximum thicknesses of 70 to 100 μm[25][26] for the Fe-Si-B amorphous alloy, 80 to 120 μm[26] for the Fe-P-C amorphous alloy and 50 μm[26] for the Co-Si-B amorphous alloy prepared by the conventional melt spinning process in which the change in the sample thickness was made by changing the original velocity of wheel. In this process, it is difficult to obtain a good contacting state between the molten alloy and the copper wheel, when the rotation speed is as low as below 500 rpm. The much worse contacting state is thought to result in the much lower critical sample thickness for glass formation. At any event, in the comparison with the maximum sample thicknesses of 70 to 100 μm for $Fe_{75}Si_{10}B_{15}$ and 80 to 120 μm for $Fe_{80}P_{13}C_7$ prepared by the conventional single roller melt spinning technique, it is concluded that the present new multicomponent Fe-based alloys have much larger glass-forming ability.

4.3. Difference in the crystallization behavior between continuous heating and cooling treatments

The crystallization of the $Fe_{72}Al_5Ga_2P_{10}C_6B_5Si_1$ amorphous alloy upon continuous heating takes place from the supercooled liquid through a single exothermic reaction accompanying the simultaneous precipitation of five crystalline phases α-Fe, Fe_3P, Fe_3B, Fe_2B and Fe_3C[18]. However, Fig. 1 shows that the preferential precipitation of Fe_3B phase takes place on the freely solidified phase of the 220 μm thick ribbon sample. The precipitation behavior is different from the heating-induced crystallization behavior in which the five crystalline phases appear simultaneously. The difference allows us to presume that the precipitation of the Fe_3B phase on the freely solidified surface takes place heterogeneously. The ease of the heterogeneous nucleation for the Fe_3B phase seems to be the reason for the difference against the heating-induced crystallization structure in which the homogeneous crystallization takes place through the simultaneous precipitation of the five crystalline phases. Although the reason for the ease of the heterogeneous nucleation of the Fe_3B phase remains unclear, it may be due to the decrease in the nucleation energy for Fe_3B phase resulting from the heterogeneous formation of an oxide surface layer.

5. Summary

With the aim of producing a thick amorphous sheet with good soft magnetic properties in Fe-based system, we examined the thermal stability of supercooled liquid, crystallization behavior and magnetic properties for the melt-spun $Fe_{72}Al_5Ga_2P_{10}C_6B_4Si_1$ amorphous sheets with different thicknesses. The results obtained are summarized as follows.

(1) The amorphous alloy sheets were formed in the thickness range up to about 200 μm. The further increase in the thickness caused the partial precipitation of Fe_3B only on the freely solidified surface, though the main constituent phase is an amorphous phase.

(2) No distinct changes in T_g, T_x and ΔT_x are seen in the thickness range up to 200 μm and the large ΔT_x of 58 K is maintained even for the 200 μm thick ribbon. The heat of irreversible structural relaxation decreases with increasing ribbon thickness and the T_c increases from 597 K for the 22 μm thick ribbon to 619 K for the 160 μm thick ribbon.

(3) In comparison with the other Fe-(Al,Ga)-(P,C,B,Si) amorphous ribbons, there is a tendency for t_{max} to increase with increasing ΔT_x. The high thermal stability of the supercooled liquid is the origin of the formation of the thick amorphous sheets.

(4) There are no distinct changes in σ_s, H_c and μ_e with ribbon thickness for the as-quenched amorphous ribbons. In the amorphous state, H_c keeps a low value of 5 A/m in the entire ribbon thickness range, but μ_e at 1 kHz decreases from 12000 for the 30 μm thick ribbon to 7000 for the 200 μm thick ribbon.

(5) The thick amorphous ribbons in the thickness range of 150 to 200 μm exhibit good soft magnetic properties of 4 to 5 A/m for H_c and about 7000 for μ_e which are much superior to those for the Fe-Si-B amorphous sheets, because of the much larger glass-forming ability.

The synthesis of the Fe-based thick amorphous sheets with the wide supercooled liquid region before crystallization and the good soft magnetic properties is important for further extension of application fields of ferromagnetic amorphous alloys.

1) T. Mizoguchi, K. Yamauchi and H. Miyajima, Amorphous Magnetism, Plenum Press, (1973), 325.
2) H. Fujimori, T. Masumoto, Y. Obi and M. Kikuchi, Jpn. J. Appl. Phys., 13(1974), 1889.
3) A. Inoue, K. Ohtera, K. Kita and T. Masumoto, Jpn. J. Appl. Phys., 27(1988), L2248.
4) A. Inoue, M. Kohinata, A. P. Tsai and T. Masumoto, Mater. Trans., JIM, 30(1989), 378.
5) A. Inoue, T. Zhang and T. Masumoto, Mater. Trans., JIM, 30(1989), 965.
6) A. Inoue, H. Yamaguchi, T. Zhang and T. Masumoto, Mater. Trans., JIM, 31(1990), 104.

7) A. Inoue, T. Zhang and T. Masumoto, Mater. Trans., JIM, 31(1990), 177.
8) T. Zhang, A. Inoue and T. Masumoto, Mater. Trans., JIM, 32(1991), 1005.
9) A. Peker and W. L. Johnson, Appl. Phys. Lett., 63(1993), 2342.
10) A. Inoue, N. Nishiyama and T. Matsuda, Mater. Trans., JIM, 37(1996), 181.
11) A. Inoue, Mater. Sci. Forum, 179-181(1995), 691.
12) A. Inoue, Mater. Trans., JIM, 36(1995), 691.
13) A. Inoue, Sci. Rep. RITU, A42(1996), 1.
14) A. Inoue and N. Nishiyama, Mater. Trans., JIM, 38(1997), No. 2, in press.
15) A. Inoue, Proc. of the 9th Int. Conf. on Rapidly Quenched and Metastable Materials, Bratislava, 1996 August, in press.
16) A. Inoue, Y. Sinohara and J. S. Gook, Mater. Trans., JIM, 36(1995), 1427.
17) A. Inoue, A. Takeuchi, T. Zhang, A. Murakami and A. Makino, IEEE Trans. Magn., 32(1996), 4866.
18) A. Inoue, A. Takeuchi, T. Zhang, A. Murakami, Mater. Trans., JIM, 38(1997), No. 2, in press.
19) A. Inoue and J.S. Gook, Mater. Trans., JIM, 36(1995), 1180.
20) Amorphous Alloys, ed. by T. Masumoto and K. Fukamichi, Agne, Tokyo (1981), p.135.
21) C.H. Smith, Rapidly Solidified Alloys, ed. H. H. Liebermann, Marcel Dekker, Inc., New York, (1993), p.617.
22) M. Hagiwara, A. Inoue and T. Masumoto, Met. Trans., 13A(1982), 373.
23) A. Inoue, M. Hagiwara and T. Masumoto, J. Mater. Sci., 17(1982), 580.
24) M. Hagiwara, A. Inoue and T. Masumoto, Mater. Sci. Eng., 54(1982), 197.
25) T. Sato, T. Yamada and T. Ozawa, MRS Int'l. Mtg. on Advanced Materials, Vol. 3, (1989), 303.
26) M. Hagiwara, A. Inoue ands T. Masumoto, unpublished research (1981).